19

Solar Wind Sails

Ikkoh Funaki[1] and Hiroshi Yamakawa[2]
[1]*Japan Aerospace Exploration Agency*
[2]*Kyoto University*
Japan

1. Introduction

Magnetic sail (MagSail) is a unique but never-realized interplanetary propulsion system. The original idea of MagSail proposed by Zubrin is depicted in Fig.1 (Andrews & Zubrin, 1990). A MagSail spacecraft has a hoop coil, and it produces an artificial magnetic field to reflect the solar wind particles approaching the coil, and the corresponding repulsive force exerts on the coil to accelerate the spacecraft in the solar wind direction. MagSail and its derivatives are usually called as solar wind sail in contrast to solar light sail, which is propelled by the solar light pressure. Before realizing the ideas of solar wind sail, however, fundamental studies are required from both physical and engineering points of view, in particular, experimental validation of these ideas are very important before applying these concepts to realistic spacecraft design.

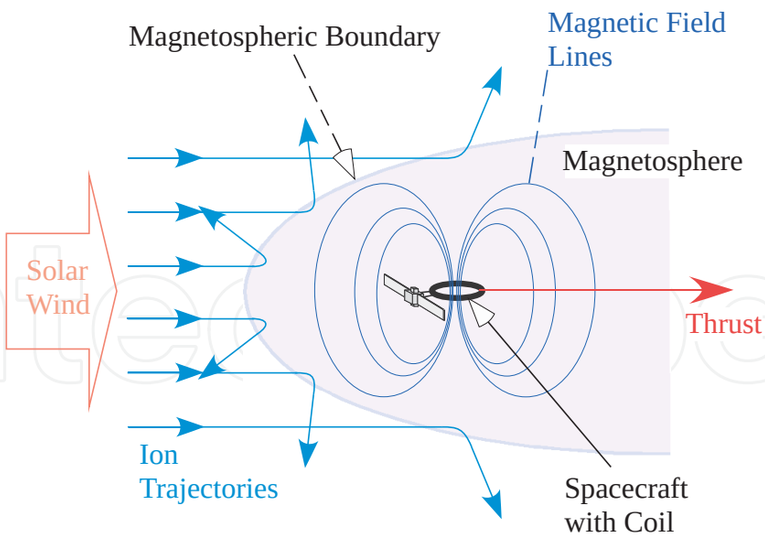

Fig. 1. Solar Wind Sail (MagSail).

To simulate a solar wind sail in laboratory, we fabricated a plasma wind tunnel facility (Funaki, 2007). Our special effort in laboratory experiment is directed to satisfy the similarity law associated with plasma flows of MagSail and its derivatives. Also, the laboratory experiment is intended for direct thrust measurement, which was never tried in the past. In

this chapter, after introducing the basics of sail propulsion using the solar wind, details of experimental facility and experimental results of MagSail in laboratory are described.

2. Principle of MagSail

In this section, the idea and feature of MagSail are introduced and its thrust formula is provided.

2.1 Original MagSail by Zubrin

In 1991, Zubrin released the idea of interplanetary MagSail, which deploys superconducting cable after launched into space (Zubrin & Andrew, 1991). Before the launch of a MagSail spacecraft, a loop of superconducting cable, which is millimeter in diameter is attached on a drum onboard the spacecraft. After launch, the cable is released from the spacecraft to form a loop of tens of kilometers in diameter, then, a current is initiated in the loop. Once the current is initiated, it will be maintained in the superconductor without operating power supply. The magnetic field created by the current will impart a hoop stress to the loop for aiding the development and eventually forcing it to a rigid circular shape.

When MagSail is operated in interplanetary space, charged particles approaching the current loop are decelerated/deflected according to the B-field they experience. If the interacting scale length between the plasma flow and the magnetic field is large as in the cases of some magnetized planets like Earth and Jupiter, a magnetosphere (a magnetic cavity or a magnetic bubble) is formed around the current loop (Fig. 2). The solar wind plasma flow and the magnetic field are divided by a magnetopause, at which ions entering the magnetic field are reflected except near the polar cusp region where the ions can enter deep into the magnetic bubble. Due to the presence of the magnetosphere, the solar wind flow is blocked, creating a drag force exerting on the loop; thus a MagSail spacecraft is accelerated in the direction of the solar wind. The solar wind in the vicinity of the Earth is a flux of 10^6 protons and electrons per cubic meter at a velocity of 400 to 600 km/s. The maximum speed available for MagSail would be that of the solar wind itself.

2.2 Thrust of MagSail

One can easily imagine that a force on the current loop depends on the area blocking the solar wind. By increasing the blocking area, a large thrust force is expected. The force on the coil of a MagSail is therefore formulated as,

$$F = C_d \frac{1}{2} \rho_{sw} u_{sw}^2 S \tag{1}$$

where C_d is thrust coefficient, $1/2\rho_{sw}u_{sw}^2$ is the dynamic pressure of the solar wind, and S is the blocking area. In Eq.(1), $\rho_{sw}=m_i n$ is the density of the solar wind, m_i is the mass of an ion, n is the number density, and u_{sw} is the velocity of the solar wind.

To calculate F from Eq.(1), the blocking area S should be specified, but S is not priori given. It is therefore customary to employ the characteristic length, L, and to approximate the blocking area as $S=\pi L^2$. In this paper, we choose the standoff distance as the characteristic

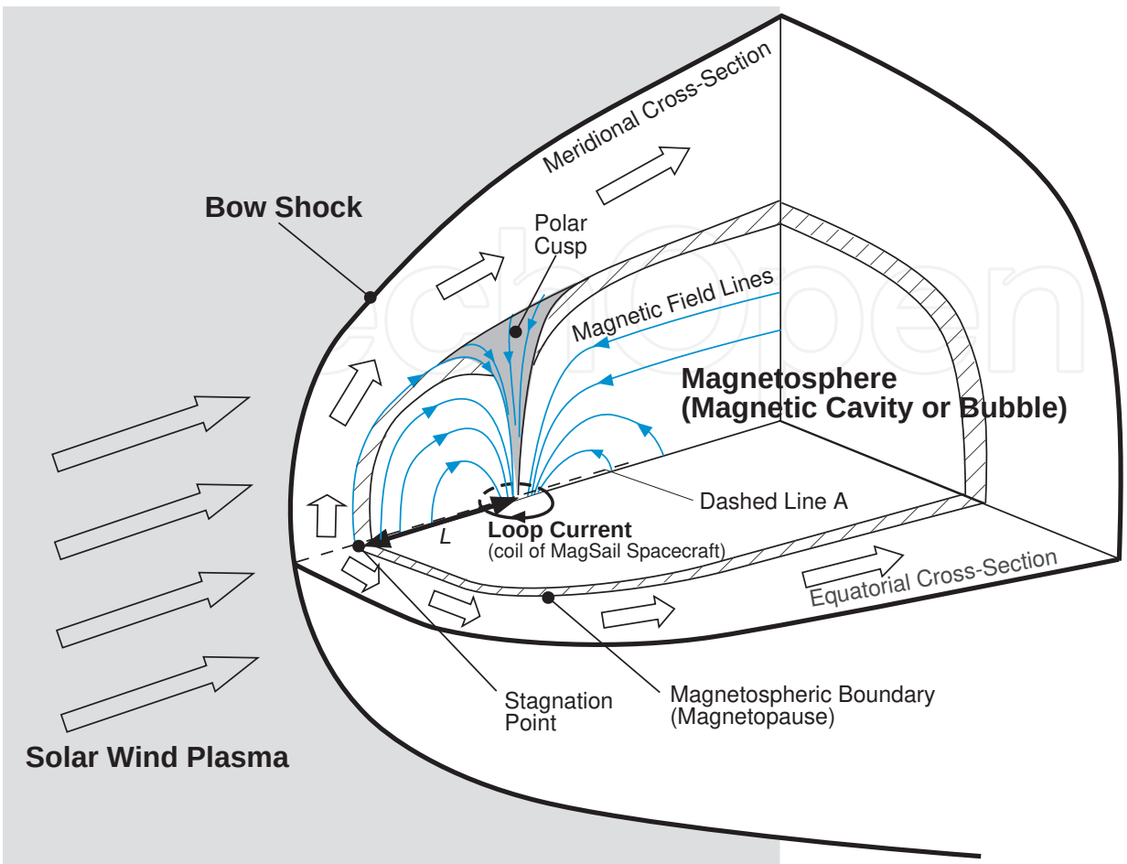

a) Magnetosphere of MagSail

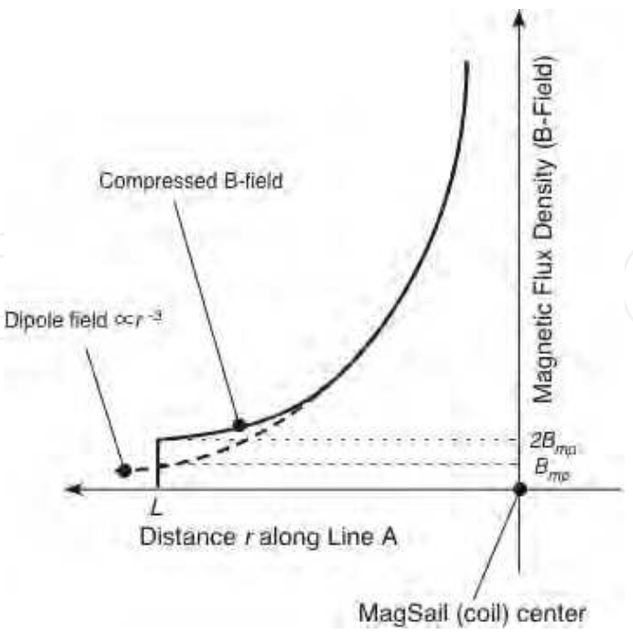

b) B-field distribution along stagnation line (dashed line A in a))

Fig. 2. Expected plasma and magnetic fields of MagSail.

length, which is the distance between the stagnation point and the center of the coil. L is derived from a pressure balance at the stagnation point (Obayashi, 1970) as

$$n m_i {u_{sw}}^2 = \frac{\left(2B_{mp}\right)^2}{2\mu_0}, \tag{2}$$

where B_{mp} is expressed using the magnetic moment, M_m, as

$$B_{mp} = \frac{\mu_0 M_m}{4\pi L^3}. \tag{3}$$

From these two equations, the standoff distance, L, is directly obtained as,

$$L = \left(\frac{\mu_0 {M_m}^2}{8\pi^2 n m_i {u_{sw}}^2} \right)^{1/6}. \tag{4}$$

Because L is uniquely determined from solar wind properties as well as the magnetic moment of MagSail, L is a reasonable choice for the characteristic length of the flow around MagSail.

Using eq.(1) and $S=\pi L^2$, the correlation between L and F is derived as

$$F = C_d \frac{1}{2} \rho u_{sw}^2 \pi L^2 \tag{5}$$

in which C_d in Eq.(5) is a fitted curve to numerical simulation results (Fujita, 2004):

$$C_d = \begin{cases} 3.6 \exp\left(-0.28 \left(\frac{r_{Li}}{L} \right)^2 \right) & for \quad \frac{r_{Li}}{L} < 1 \\ \frac{3.4}{(r_{Li}/L)} \exp\left(-0.22 \left(\frac{L}{r_{Li}} \right)^2 \right) & for \quad \frac{r_{Li}}{L} \geq 1 \end{cases} \tag{6}$$

where r_{Li} is ion's Larmor radius defined afterwards. Thrust by Eqs.(5) and (6) is plotted in Fig.3 The MagSail by Zubrin (Zubrin & Andrews, 1991) required a spacecraft with a large

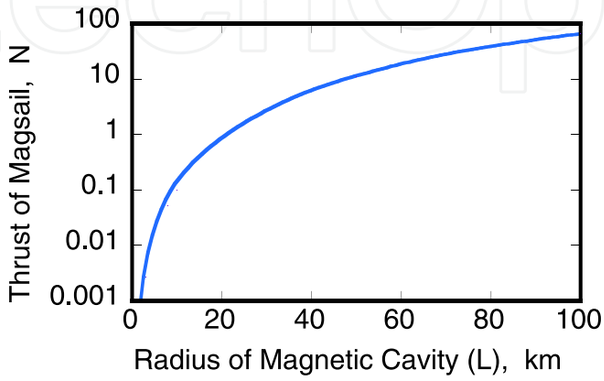

Fig. 3. Theoretical prediction of thrust by MagSail.

hoop coil of 64 km in radius to form 100-km-radius blocking area (which corresponds to approximately 30-N-class thrust). However, the dimension of the hoop coil was too large to realize. We therefore try to design a smaller MagSail than Zubrin proposed. From Fig. 3, one may notice that for L=20 km, 1 N is obtained. We selected the target of MagSail as 1 N, which corresponds to L=20 km; this is an adequate thrust level for medium-size (1,000-kg-class) deep space explorers.

2.3 Scaling parameters of MagSails

Empirical equation (6) indicates that thrust by MagSail is significantly influenced by the non-dimensional parameter, r_{Li}/L. In this section, similarity law for MagSail is explained after introducing two important scaling lengths, ion Lamor radius and skin depth.

2.3.1 Ion Larmor radius and skin depth

The boundary between a solar wind plasma and a magnetosphere is called magnetospheric boundary or magnetopause, where induced currents divide the plasma and the magnetic field regions. Magnetospheric boundary is schematically plotted in Fig.4. As in Fig.4, when charged particles impinge on the magnetospheric boundary from outside the magnetospheric boundary, ions can enter deep into the magnetosphere, whereas electrons are trapped and they are reflected back to the sun direction at the surface of the boundary. It is expected that the penetration depth of ions is comparable to ion Larmor radius:

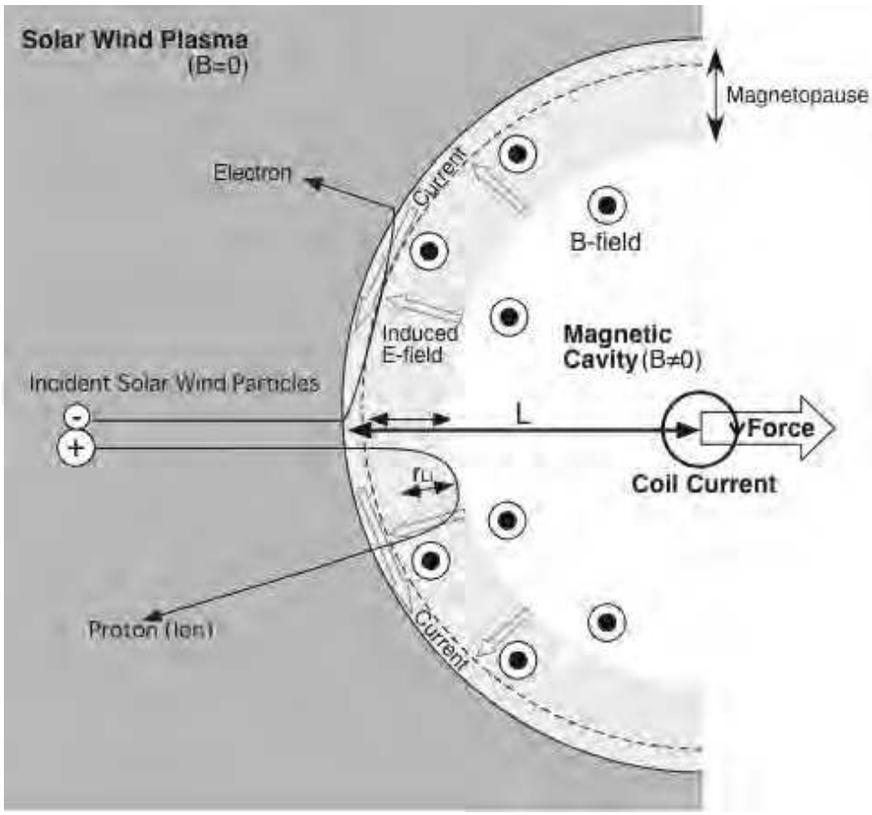

Fig. 4. Charged particle behaviour near magnetopause.

$$r_{Li} = \frac{m_i u_{sw}}{e \cdot 2B_{mp}} \tag{7}$$

from which r_{Li}=72 km if we put m_i=1.67x10^{-27} kg, u_{sw}=400 km/s, e=1.6x10^{-19} C, and B_{mp}=29 nT.

Disparity between ion's and electron's penetration depth at this boundary will also cause charge separation; this sheath region will induce an outward electric field. By this electric field, an electron is accelerated to a high velocity, resulting in a motion with large Larmor radius in the magnetosphere. Such electron motion dominates magnetospheric current at the outer edge of the magnetopause. In contrast to the electron motion at the boundary, ions are decelerated by the same electric field. The theoretical length of charge separation is the skin depth:

$$\delta = c/\omega_p \tag{8}$$

which is the decaying length of an electromagnetic wave incident on a plasma (Bachynski & Osborne, 1965); in eq.(8), c is the light speed and ω_p is the plasma frequency. For the solar wind plasma, δ ~1 km. Realistic penetration depth takes a value between δ and r_{Li} when background neutralizing electrons reduce the magnitude of the outward electric field (Nishida, 1982).

2.3.2 Non-dimensional scaling parameters of MagSail

In the following, four non-dimensional parameters and similarity law for MagSail in space are obtained in analogy to the similarity law of geo-magnetophysics (Bachynski & Osborne, 1965). The solar wind is a super sonic plasma flow, and it consists of collisionless particles: typical mean free path of the solar wind is about 1 AU. These features are described by high Mach number, M > 1 as well as very high magnetic Reynolds number, Rm >>1. M and Rm are defined as follows:

$$M = \frac{u_{sw}}{\sqrt{\gamma R T_{sw}}} \tag{9}$$

$$Rm = \sigma \mu_0 u_{sw} L \tag{10}$$

where σ is electric conductivity, R is gas constant, γ is specific heat ratio, and μ_0 is permeability in vacuum. Putting typical plasma velocity and temperature of the solar wind (u_{sw}=400 km/s and T_i~10 eV) into the above equation, M~8 is obtained. Also, the assumption of Coulomb collision gives σ =2x10^4/Ωm and Rm~10^8 for L=10 km. In addition to these two non-dimensional parameters, we defined r_{Li}/L, and δ/L, hence four non-dimensional parameters in total are introduced and they are listed in Table.1. Among them,

Parameters	MagSail	
	in space	in laboratory
Mach number	~ 8	> 1
Ratio of ion larmor radius to L (r_{Li}/L)	~ 1	~ 1
Ratio of skin depth to L (δ/L)	< 1	< 1
Magnetic Reynolds' number (Rm)	~10^8	~ 10

Table 1. Non-dimensional parameters of MagSail.

the parameters Rm, r_{Li}/L, and δ/L, are functions of the size of the magnetosphere, in which L was selected as 10 km<L< 100 km in our study. Corresponding non-dimensional parameters are $0.72 < r_{Li}/L < 7.2$ (the ion gyration radius is comparable to or larger than L), which is in contrast to the MHD scale requiring $r_{Li}/L << 1$), and lastly, $\delta/L < 0.03$ (the skin depth is much smaller than L).

Since $\delta << r_{Li}$, the effective thickness of magnetopause is considered to be r_{Li}. As shown in Fig.5, if the thickness of the magnetopause is small enough in comparison to L, almost all of the incident ions are reflected at the magnetospheric boundary, hence large thrust on the coil of the MagSail is expected. Vice versa, if the thickness of the magnetopause is much larger than L, no interaction between the plasma flow and the magnetic field is anticipated. We treat a transitional region from the MHD scale (thin magnetopause mode) to the ion kinetic scale (thick magnetopause mode) in this experiment.

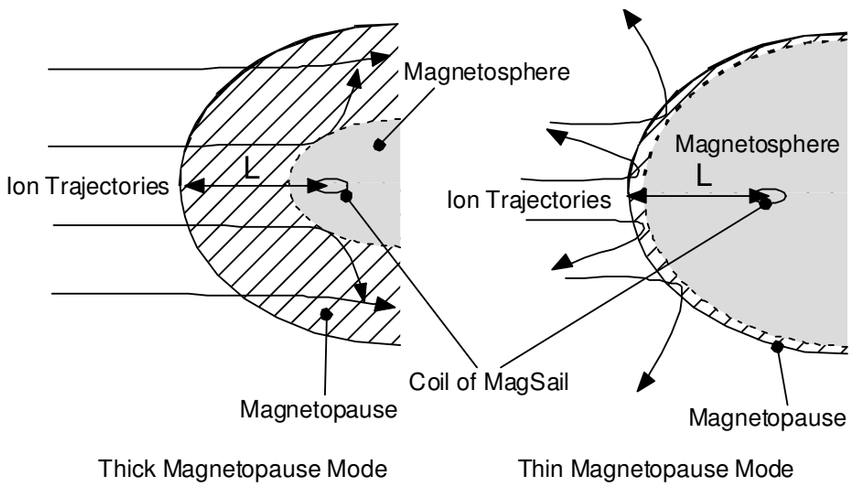

Fig. 5. Thick and thin magnetopause of MagSail.

3. Experimental setup for MagSail

Based on the above scaling consideration, experimental setup for MagSail is developed (Funaki, et al., 2006). The setup consists of a high-power solar wind simulator and a coil simulating MagSail spacecraft, both of which are operated in a quasi-steady mode of about 0.8-ms duration. In our experiment of MagSail (Fig.6), a coil simulating MagSail spacecraft (20-75 mm in diameter) was located at a downstream position of the solar wind simulator, and a plasma jet was introduced to a magnetic field produced by the coil. Typical snapshot is shown in Fig.7, in which plume jet as well as the coil simulating MagSail can be found.

A magnetoplasmadynamic (MPD) arcjet in Fig.8 was used as the solar wind simulator (SWS). The discharge chamber of the MPD arcjet is 50 mm in inner diameter and 100 mm in length. The MPD arcjet consists of eight molybdenum anode rods (8 mm in diameter) azimuthally located, and a short thoriated tungsten cathode rod 20 mm in diameter; they are surrounded by an annular floating body and insulators. These electrodes enable stable operate from a low current discharge range to an erosive high current discharge range. The SWS is attached on the space chamber inner wall as shown in Fig. 6.

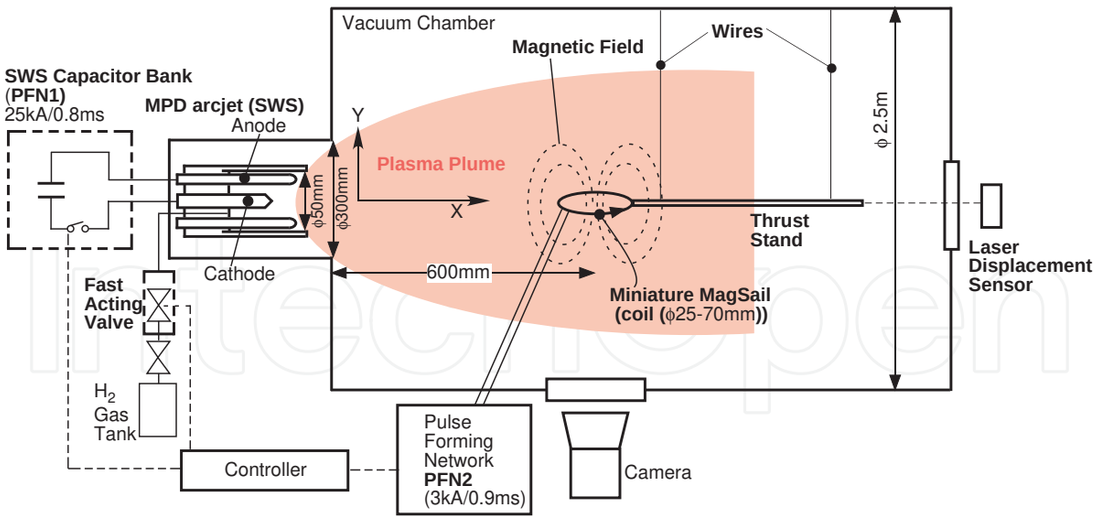

Fig. 6. Schematics of MagSail experimental facility.

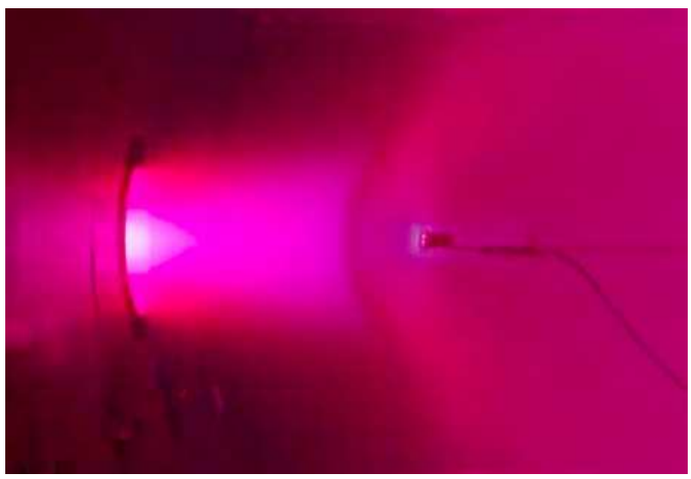

Fig. 7. Experiment of MagSail; typical snap shot.

Fig. 8. Magnetoplasmadynamic(MPD) arcjet as solar wind simulator (SWS).

A fast-acting valve (FAV) allowed us to feed gaseous propellants to the MPD arcjet. The hydrogen mass flow rate was controlled by adjusting the reservoir pressures. Timing of experiment is explained in Fig.9. After a gas pulse reaches its quasi-steady state, a pulse-forming network (PFN) is triggered. The PFN for SWS supplies the discharge current up to 20 kA with a flat-topped waveform in quasi-steady mode as shown in Fig.9. PFN for the coil (PFN2) supplies rather small current below 3 kA, and 20- to 75-mm-diameter 20-turn coil is required to produce up 2.0-T B-field at the center of the coil. After coil current (MagSail operation) reaches its steady state, discharge of the SWS (MPD arcjet) is initiated.

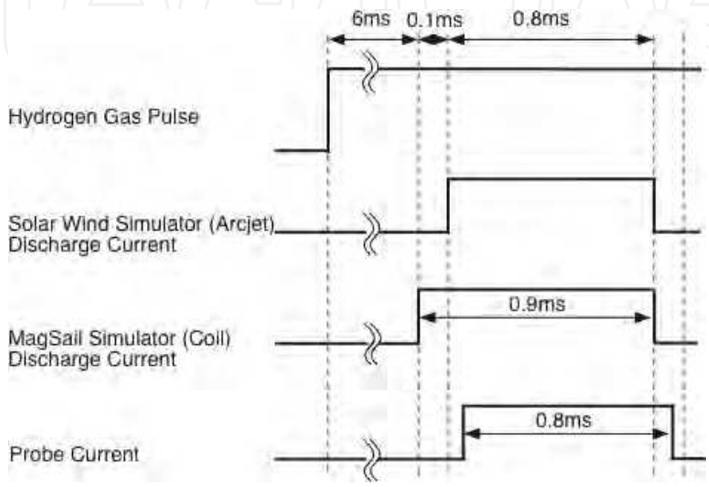

Fig. 9. Timing of MagSail experiment.

4. Experimental results of MagSail

In this section, after operational characteristics of MagSail in laboratory are described, thrust measurement results are provided. Then, the similarity law on a plasma flow of MagSail is discussed.

4.1 Operation of MagSail in lab

Discharge current profiles of the solar wind simulator (SWS) MPD arcjet and the coil are plotted in Fig.10. Flat-topped quasi-steady discharge continues about 0.8 ms in the case of SWS, and 1.0 ms in the case of the coil simulating MagSail spacecraft. High speed photos of MagSail experiment are shown in Fig.11. After the coil current (MagSail operation) reach its steady state, discharge of the MPD arcjet is initiated (Fig.11(a)). In Figs.11(b) and (c), it is observed that a wave front expands radially. This shock wave is followed by a quasi-steady plasma flow, that interacts with the magnetic field created by the solenoidal coil (Fig.11(d)).

During the quasi-steady interaction (0.25-1.0 ms in Fig.10), it was found that the plasma flow at the coil position was fluctuating. Averaged plasma parameters during the quasi-steady interaction were evaluated by Langmuir probe diagnostics as well as time-of-flight velocity measurement at the coil position. Results are listed in Table.2. The size of SWS's plume is 0.7 m in diameter (FWHM) at the coil position, and it is adequate for the laboratory experiment of Magnetic sail, which has typically 10-cm-size magnetic cavity. Scaling parameters can be calculated from the measurement in Table.2, but they are discussed afterwards in this chapter.

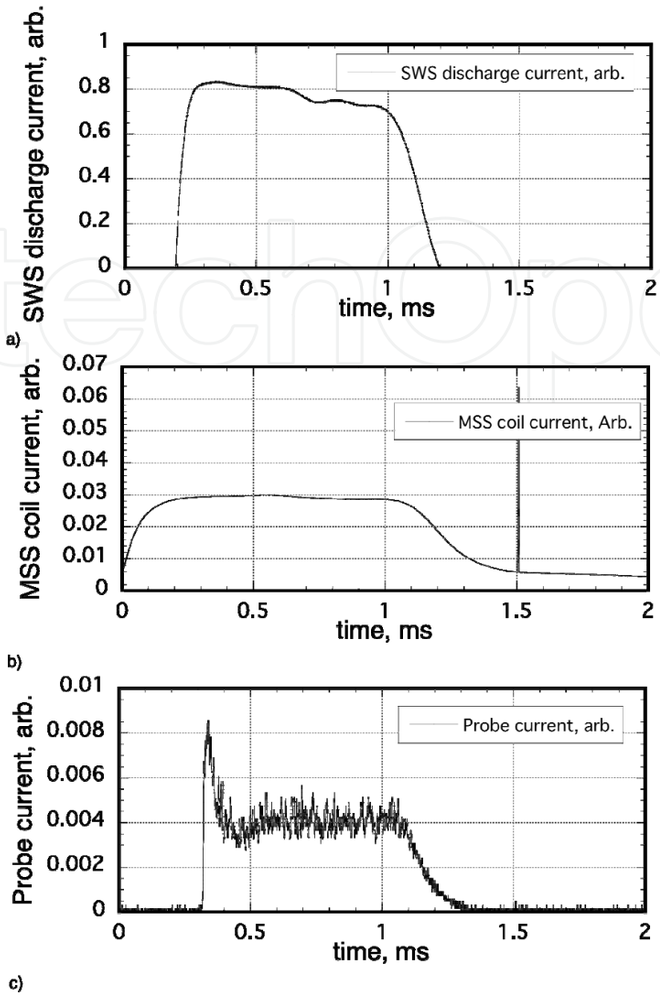

Fig. 10. Operation of solar wind simulator; a) discharge current profile of SWS, b) coil current profile, and c) plasma plume probe current profile (ion saturation current) at the coil position for H_2 0.4 g/s, charging voltage of PFN for SWS is 4 kV, and charging voltage of PFN for coil is 1.5 kV.

Plasma stream form hydrogen MPD solar wind simulator	
Velocity	20–45 km/s
Plasma density	10^{18}–10^{19} /m^3
Electron temperature	1 eV
Radius of plasma stream at the coil position	0.2–0.35 m
Plasma duration	0.8 ms
Coil current simulating MagSail in operation	
Radius of coil	9-37.5 mm
B-field at the center of coil	0–2.0 T
Duration of exciting current	0.9 ms

Table 2. Operating conditions and plasma parameters of solar wind simulator and coil simulating MagSail spacecraft.

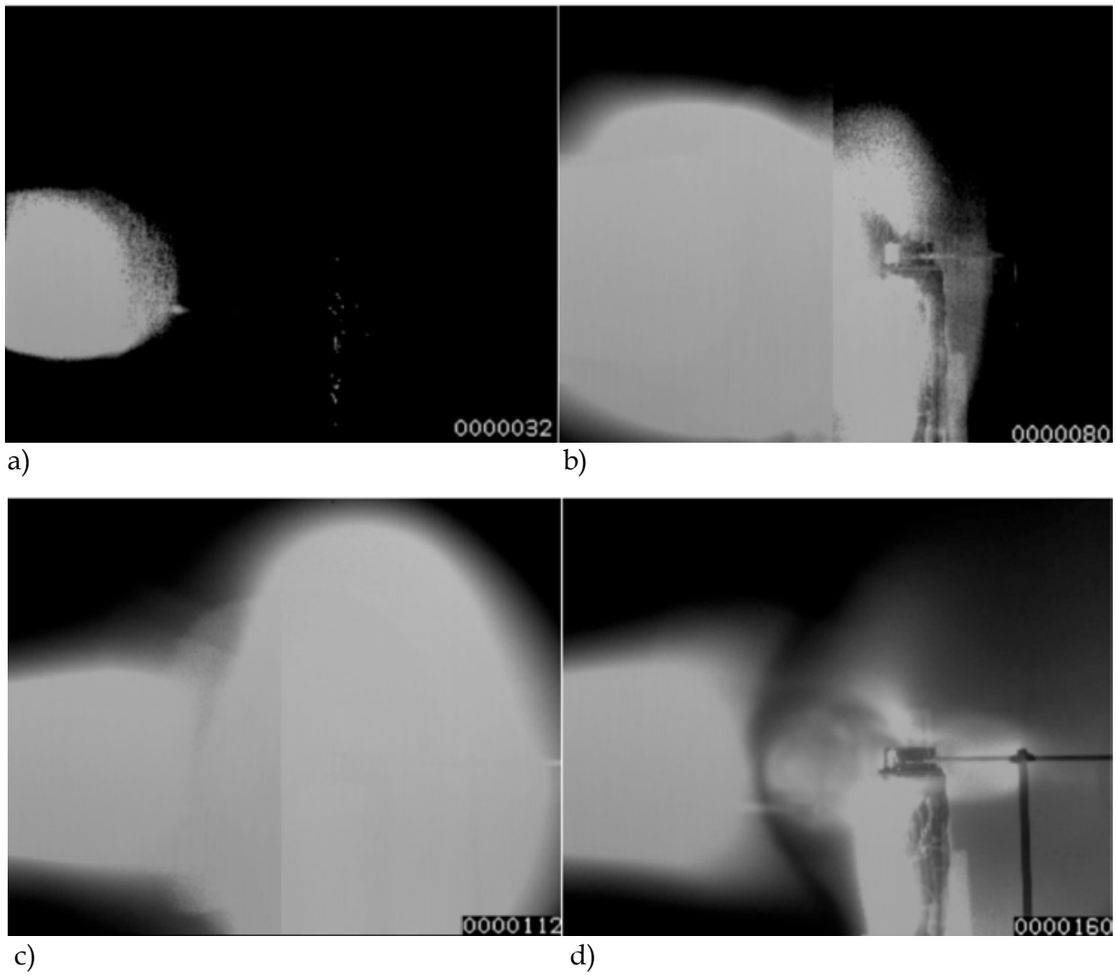

Fig. 11. High speed photos of pure MagSail experiment; a) just after initiating SWS (t=32 μs has passed after the discharge is initiated), b) t=80 μs, c) t=112 μs, and d) t=160 μs; d) corresponds to a quasi-steady state operation) in the case of 45 km/s, $2x10^{19}$ m^{-3} plasma flow from SWS, B-field at the center of coil is 1.8 T.

Another view of MagSail experiment is shown in Fig.12, in which a shutter camera was used to capture MagSail and its flowfield during a quasi-steady interaction. The most important feature of the interaction is the magnetospheric boundary between the SWS plasma flow and the low-energy plasma in the magnetic cavity. At the location of magnetospheric boundary, significant change of the magnetic field strength was found by a magnetic field measurement using a magnetic probe (Ueno, et al, 2009).

As far as we see Fig.12, the interaction seems very stable during quasi-steady operation of MagSail. However, if we see them with a high-speed camera, oscillatory magnetic cavity was observed (Oshio, et al., 2007; Oshio, et al., 2011). Thrust is hence produced under turbulent environment. Figure 13 shows high-speed photos when the discharge current of the MPD arcjet (J_{SWS}) is 11.6 kA. In Fig. 13, t = 0 corresponds to the time initiating the discharge of the SWS, and the time difference between each frame photograph is 2 μs, and shutter time is 0.5 μs. The interaction has already reached quasi-steady state in Fig. 13, in

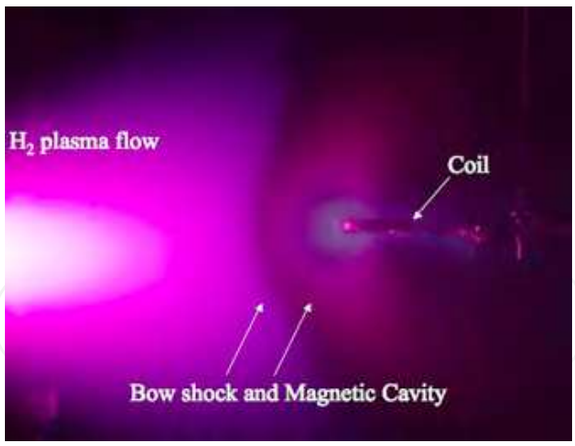

Fig. 12. Typical flow around MagSail during quasi-steady operation.

spite, an oscillating magnetosphere and plasma plume was observed. For example, when comparing the photos at 506 μs and at 516 μs in Fig. 13, the magnetospheric boundary is different. Also, when we see them in a longer time scale, it is found that the magnetospheric size shrinks and expands by about 20% repeatedly, and the averaged magnetospheric size is 0.15 m in the case of Fig. 13.

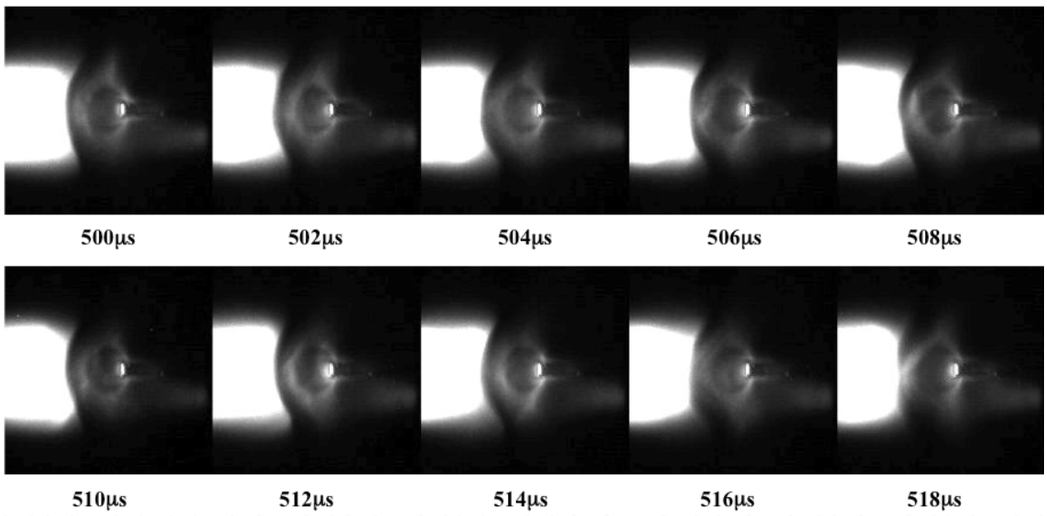

Fig. 13. High-speed photos of Magsail's magnetosphere during its quasi-steady operation; time corresponds to elapsed time after discharge of SWS is initiated. (J_{sws}=11.6 kA, J_{coil}=2 kA).

This magnetospheric fluctuation is characterized by high-speed photography based on the fact that the location of magnetopause corresponds to the dark regions in photos. Figure 14 shows the fluctuation of magnetospheric size for two plasma parameters (the discharge currents of SWS are 7.1 kA and 11.6 kA). The magnetospheric size is defined as a distance from coil center to the dark region. The averaged magnetospheric size is 145 mm in Fig.14a), and 80 mm in Fig. 14b). The magnetospheric size for J_{sws}=11.6 kA is larger than the case for J_{sws} =7.1 kA by about 10 mm, because the dynamic pressure of the simulated solar wind is smaller. The amplitudes of these fluctuations are about 10 mm, which corresponds to the fluctuation of thrust of about 25%. The power spectrum densities show that the dominant

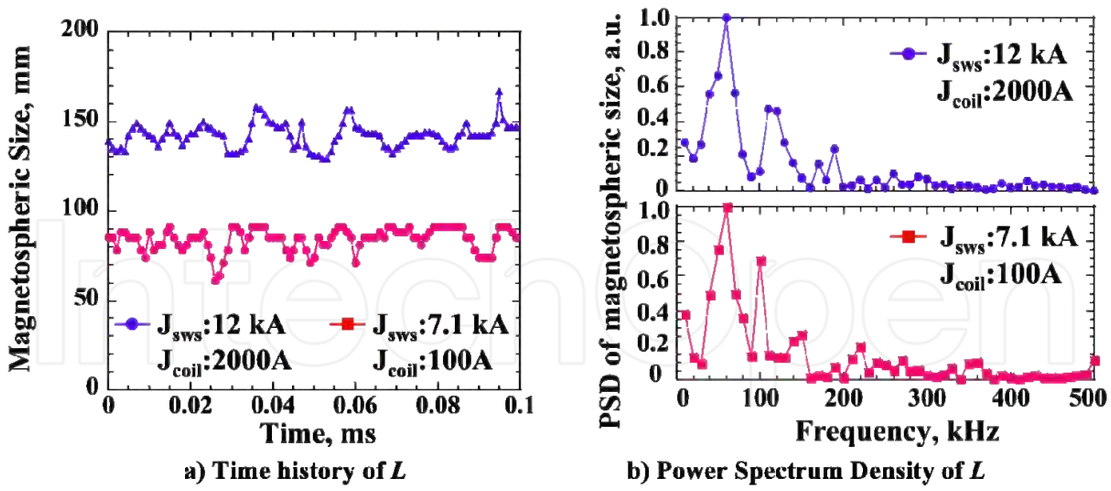

Fig. 14. Magnetospheric size (L) fluctuation of Magsail; obtained from image analysis.

frequency was about 60 kHz. This frequency corresponds to a natural mode of bouncing magnetosphere. Such a bouncing magnetosphere is also expected in space in a frequency range of 1-10 Hz in the case of moderately sized MagSail (L~100 km).

4.2 Thrust measurement of MagSail

The magnetic cavity is blocking the plasma flow emitted from the MPD arcjet to produce a force exerting on a miniature MagSail spacecraft (coil). To evaluate this solar wind momentum to thrust conversion process, impulse measurements were carried out by the parallelogram-pendulum method (Ueno, et al., 2009; Ueno, et al., 2011). For the measurement, a coil simulating MagSail was mounted on a thrust stand suspended with four steel wires as shown in Fig.6.

The impulse of a Magnetic Sail is given by the following equation:

$$(F\Delta t)_{MagSail} = (F\Delta t)_{Total} - (F\Delta t)_{SWS} \tag{11}$$

When only the solar wind simulator is operated, the pressure on the coil surface produces impulse; this impulse corresponds to $(F\Delta t)_{SWS}$ in Eq. (5). If the coil current is initiated during the solar wind operation, the impulse, $(F\Delta t)_{Total}$, becomes larger than $(F\Delta t)_{SWS}$. Thrust by a Magnetic Sail is defined as the difference between the two impulses divided by the SWS operation duration (Δt = 0.8 ms):

$$F_{MagSail} = \frac{(F\Delta t)_{MagSail}}{\Delta t} \tag{12}$$

In the experiment, the displacement of the pendulum was measured with a laser position sensor. For the calibration of the pendulum and position sensor combination, impulses of known magnitude were applied to the coil simulating MagSail.

Displacement waveforms of the thrust stand were observed as in Fig.15 when a coil was immersed into the plasma flow. We can see that the maximum displacement for 1.1-kA coil

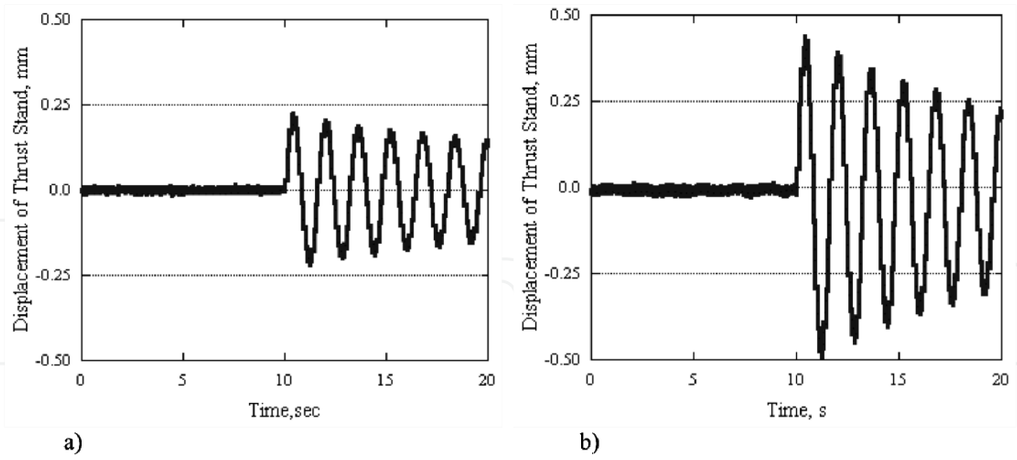

Fig. 15. Thrust stand's swing when 25-mm-diameter coil was immersed into hydrogen plasma flow (u_{sw}=47 km/s, n=1.8x10^{19} m^{-3}); a) without coil current, and b) 1.1 kA coil current (Simulator was initiated at 10s).

current in Fig.15b) is about two times larger than that without a coil current in Fig.15a). Figure 16 shows thrust data of MagSail for various magnetic moments where the magnetic moments were derived from the coil geometry and the coil current. It was confirmed that the thrust level is increased when increasing the magnetic moment of coils and thrust is proportional to $(M_m)^{2/3}$, which is consistent with eq.(5) because $L \propto (M_m)^{1/3}$.

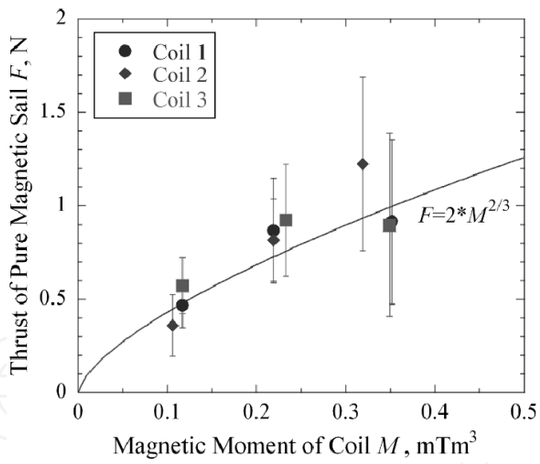

Fig. 16. Thrust vs. magnetic moment in the case of MagSail; SWS was operated for hydrogen plasma flow (u_{sw}=47 km/s, n=1.8x10^{19} m^{-3}), and three types of coils (radius=25 mm (coil 1,2) or 35 mm (coil 3)) are positioned at X=0.6 m.

If ions in a solar wind plasma penetrate into the magnetic cavity, the ions experience Larmor gyration. As was shown in Figs.4 and 5, if $r_{Li}<L$ at magnetospheric boundary, ions are reflected, but if $r_{Li}>L$, ions will not be reflected at the magnetospheric boundary but will penetrate deep into the magnetic cavity without producing thrust by MagSail. As a result, small $r_{Li}<L$ is required to obtain a significant thrust level. Such trend can be summarized in Fig.17, in which C_d (non-dimensional thrust) becomes smaller at a higher r_{Li}/L value.

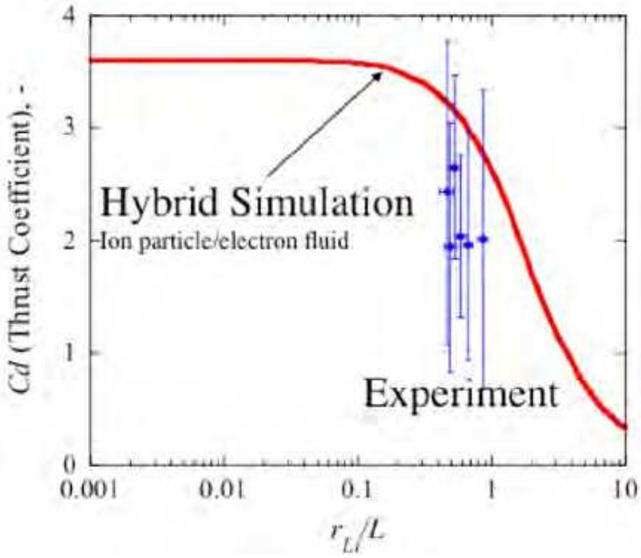

Fig. 17. Non-dimensional thrust characteristics of MagSail; C_d for various r_{Li}/L.

Through the experiment of MagSail, MHD to ion scale MagSail (r_{Li}/L=0.1~1.0) was demonstrated in laboratory.

Seeing the detail of Fig.17, however, one can see that laboratory experiment shows rather small thrust level than that by numerial simulation. This discrepancy is caused as a result of the collisional effect that is inevitable in laboratory [Kajimura et al., 2010], and it means that the laboratory experiment cannot predict the entire feature of collisionless plasmas in space. In the laboratory experiment, the momentum of a plasma flow in a vacuum chamber decreases as a result of collisions with neutral particles, leading to a decrease in thrust level.

4.3 Checking the similarity law

As described before, laboratory experiment is prepared so that the plasma flow follows the similarity law of MagSail/MPS in space. In the following, similarity law including the collisional effect in laboratory is checked based on measured plasma parameters.

When the hydrogen propellant is ionized, protons without a bounded electron are produced. Most of the plume plasma jet released from the SWS-MPD consists of atoms and protons, but molecules are minor species. By estimating the degree of ionization, the scaling parameters in our scale model are to be discussed.

From the data in Table.1, the radius of the plume plasma was 0.35 m at the coil position (X=0.7 m), which indicates that the plume divergence angle was 45 degree. The mass flow rate of a plasma jet from the MPD arcjet is the sum of a neutral flow rate and an ion flow rate,

$$\dot{m} = \left(m_n n_n u_n + m_i n_i u_i \right) A \tag{13}$$

From eq.(13), n_n=1.7x10^{19} m^{-3} is obtained for $\dot{m}$ =0.4 g/s, u_n=u_i=45 km/s, and the cross-sectional area of SWS's plume A= π (0.35)^2 m^2. In a realistic MPD arcjet flow, however, the velocity slip between the ions and the atoms are usually found. Including this effect, n_n=3.4x10^{19} m^{-3} for u_i=45 km/s, and u_n= 22.5 km/s. This estimation gives ionization ratio

α=0.2. Using the obtained species concentrations, the mean free paths can be calculated, and an example is shown in Table 3 for typical operational parameters of SWS.

Variable		Expression or assumption	Value
Electron density	n_e	measured typical value	2.0×10^{18} m^{-3}
Electron temperature	T_e	measured typical value	11640 K
Ion/atom temperature	T_i	$T_i \approx T_e$ is assumed	11640 K
Ion velocity	u_i	measured typical value	45 km/s
Thermal velocity	$u_{th,e}$	$\sqrt{8kT_e/m_e\pi}$	6.7×10^5 m/s
	$u_{th,i}\left(\approx u_{th,n}\right)$	$\sqrt{8kT_i/m_i\pi}$	1.6×10^4 m/s
Size of magnetic cavity	L	design value	0.1 m
Mean free path	λ_{ei}	$u_{th,e}/\nu_{ei}$	0.012 m
	λ_{en}	$1/n_n\sigma_{en}$	0.074 m
	λ_{nn}	$1/\sqrt{2}n_n\pi d^2$	0.60 m
Collision frequency	ν_{ei}	$3.64\times10^{-6}n_e\ln\Lambda/T_e^{3/2}$	5.4×10^7 /s
	ν_{en}	$u_{th,e}/\lambda_{en}$	9.1×10^6 /s
	ν_{nn}	$u_{th,n}/\lambda_{nn}$	2.6×10^4 /s
Electric conductivity	σ	$n_e e^2/m_e\left(0.51\nu_{ei}+\nu_{en}\right)$	2040
Non-dimensional variables		Expression	Value
Knudsen Number	(electron-ion)	λ_{ei}/L	0.12
	(electron-atom)	λ_{en}/L	0.74
	(atom-atom)	λ_{nn}/L	6
Magnetic Reynolds Number	Rm	$\sigma\mu_0 u_i L$	12

Table 3. Operational, measured, and scaling parameters of MagSail in laboratory.

In this experiment, coil diameter (18 mm) and magnetospheric size (L~100 mm) are smaller than the mean free path of hydrogen atoms, hence neutral flow behaves as collisionless particles. Proton and hydrogen atoms also behave as collisionless particles, but electron-heavy particle collision is significant and hence the mean free path of electrons is smaller than L. Let's consider electron motions in laboratory experiment. An electron coming into the magnetosphere is trapped in the magnetosphere, and then it makes a mirror movement in a magnetic flux tube. During such a mirror motion, an electron moves to another magnetic flux tube as a result of a collision with a heavy particle, or completely released from the magnetosphere. Such diffused electron motions will change the skin depth of a magnetopause from δ to δ_D (Bachynski & Osborne, 1965)

$$\delta_D = \frac{c^2\left(0.51\nu_{ei}+\nu_{en}\right)}{\omega_p u_{sw}} \tag{14}$$

It is derived that the ratio of δ_D to L is equal to the reciprocal of Rm as

$$\frac{\delta_D}{L} = \frac{1}{Rm} \tag{15}$$

Also, converting the mean free path data to collision frequencies, electric conductivity is evaluated as

$$\sigma = \frac{e^2 n_e}{m_e\left(0.51\nu_{ei} + \nu_{en}\right)} \tag{16}$$

where ν_{ei} is electron-ion collision frequency and ν_{en} is electron-neutral collision frequency. Using the values in Table.3, σ is calculated as $2040/\Omega$m; then Rm=12 is obtained for u_i=45 km/s and L=0.1m. In this case, the conditions for Rm (Rm>>1) and δ_D/L <<1 are satisfied.

By further tuning SWS (by increasing Rm) more suitable plasma flow for MagSail in laboratory might be provided. To further enlarge Rm, n_n should be decreased and T_e should be increased (see the equations in Table.3).

5. Extension of MagSail: M2P2 and magnetoplasma sail

5.1 The principle of M2P2 and magnetoplasma sail

For a MagSail in space, we must create a large magnetosphere to produce a significant thrust level because the dynamic pressure of the solar wind is very small even around the Earth. Using eqs.(4) and (5), thrust level of Magsail F is rewritten as

$$F = C_d \frac{1}{4}\left(\rho u_{sw}^2\right)^{5/3}\left(\pi\mu_0\right)^{1/3} \cdot {M_m}^{2/3} \tag{17}$$

This equation shows that F is proportional to $(M_m)^{2/3}$, where $M_m = \mu_0 nJ\pi r_c^2$ is the magnetic moment. Hence, a coil with a large diameter (r_c), a high current (J), or many turns (n) are required to obtain a high thrust level. In the case of MagSail, a large magnetosphere might be formed using a coil of several tens of kilometer in diameter; for example, Zubrin proposed 10-N-class MagSail spacecraft equipped with a 64-km-diameter coil. This design is, however, impractical at the current technology level.

In order to overcome this issue, the idea to make a large magnetosphere by a compact coil diameter (~several meters) with a plasma jet was proposed instead of employing a large-scale coil. This propulsion system, illustrated in Fig.18, is called mini-magnetospheric plasma propulsion (M2P2) or MagnetoPlasma Sail (MPS). This idea gained great interest because the study by Winglee et al. (Winglee, et al., 2001) suggested the possibility of dramatically large acceleration by M2P2 spacecraft in deep space.

The M2P2/MPS sail uses an artificially generated magnetic field, which is inflated by the injection of high- or low-energy plasma. As shown in Fig.19, based on either magnetic field inflation concept either by high-velocity plasma jet or by equatorial ring-current, either of which initiates additional plasma current inside a magnetosphere to increase the magnetic moment of the system. Magnetic field inflation by plasma jet is carried out when a collisionless plasma jet is introduced in a magnetic field, and magnetic field is frozen into the plasma flow so that the plasma flow expands the magnetic field. In contrast to the method

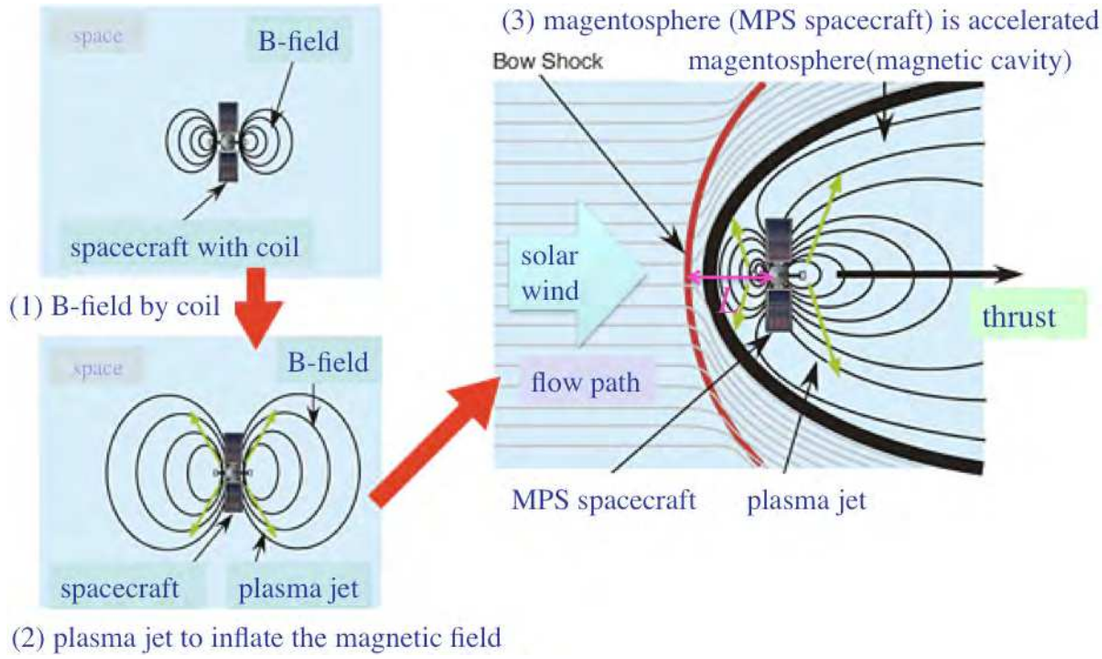

Fig. 18. M2P2/MPS concept.

using a radial flow continuously flowing out, when a low-energy plasma is trapped in the magnetosphere, equatorial ring-current is initiated due to drift motions of both ions and electrons. These plasma currents may allow the deployment of the magnetic field in space over large distances (comparable to those of the MagSail) with the B-field strengths that can be achieved with existing technology (i.e., conventional electromagnets or superconducting magnets). Additionally, one potential significant benefit of the M2P2/MPS would be its small size of the hardware (even though the magnetic bubble is very large); this would eliminate the need for the deployment of large mechanical structures that are presently envisaged for MagSail or solar light sails (Frisbee, 2003, Yamakawa, et al., 2006).

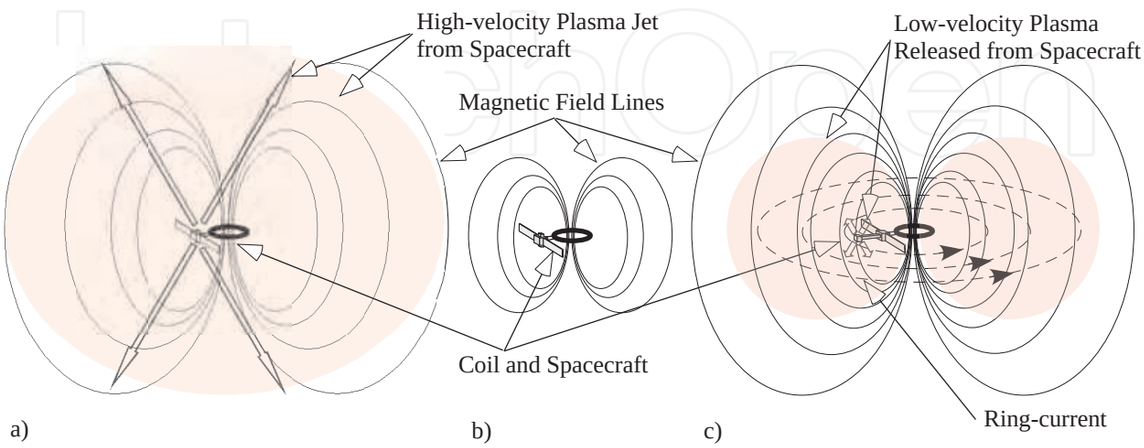

Fig. 19. Magnetic field inflation concept by high-velocity plasma jet or by equatorial ring-current.

However, feasibility of the M2P2/MPS sail concept is not established yet (Khazanov, et al., 2005; Omidi & Karimabadi, 2003}. From the physical point of view, we have questions on the principle of thrust production: under what operational condition is the M2P2/MPS concept valid?; is efficient thrust production really possible for M2P2/MPS? These are still open questions. Also, from the spacecraft design point of view, it is not known that if M2P2/MPS obtains much higher acceleration than that of existing technology such as electric propulsion or solar sail. We are continuing our efforts on theoretical and experiment studies to reveal these issues.

5.2 Preliminary experiment of M2P2/MPS

In contrast that a lot of experiments revealed the physics and thrust characteristics of MagSail, only a few data are available in the case of M2P2/MPS. The first experiment on the magnetic field inflation concept was tried by Winglee and his group (Winglee, et al., 2001; Ziemba, et al., 2001; Slough, et al., 2001; Ziemba, et al., 2003; Giersch, et al., 2003). A high-density helicon or an arc plasma source is located in a drum-like solenoid to observe magnetic field inflation. The demonstration was conducted in a space chamber of 1 m in diameter. He also tried full demonstration of M2P2. However, due to facility limitaion, they cannot demonstrate some important features of M2P2; for example, 1) the entire interaction of M2P2 is not tested due to limited diameter of the solar wind simulator, and 2) what amount of momentum transfers from the solar wind to the spacecraft (coil) are not validated.

Scaled down model approach by our group with a very small plasma source from the center of the coil seems reasonable to simulate the whole system of a M2P2/MPS sail. In Fig.20, an experimental system for MPS is depicted, which consists of a high-power magnetoplasmadynamic (MPD) solar wind simulator (MPD_SWS) and a miniature MPS spacecraft (Funaki, et al., 2007, Ueno, et al., 2009). Close-up views around the miniature MPS spacecraft (scale model) are shown in Fig.21. The miniature MPS spacecraft has a solenoidal coil and MPD arcjets (MPD_Inf, 20-mm-diameter small MPD arcjets) for plasma jet injection. All of these devices (the MPD_SWS, the MPD_Inf, and the coil) are operated again in a quasi-steady mode of about 1 ms duration. To describe the physics of the magnetic field inflation process, the most important parameter is r_{Li}/L_{inf}. In this parameter, L_{inf} is the frozen-in point where local β value is unity, so the B-field inflation occurs. Strictly speaking, L_{inf} is defined as a distance from the coil center to a typical frozen-in point. Also, the B-field inflation process requires small ion gyration radius when the B-field inflation is possible in the MHD approximation. Hence, two inequalities, $r_{Li}/L_{inf} < 1$ and $L_{inf} < L$, are added to the inequalities in Table.1. In our preliminary experiment, the miniature MPS spacecraft with a coil of 50-75 mm in diameter was located in a downstream position of the MPD arcjet (SWS) to produce up to 2-T magnetic field at the center of the coil. Into this magnetic field produced by the miniature MPS spacecraft, a plasma jet from the MPD_SWS was introduced to see possible interaction.

Typical snapshot of MPS experiment is shown in Figs.22 and 23. It is obvious that the incoming solar wind plasma flow is blocked by the magnetic cavity in both the MagSail mode as shown in Fig.23(a) and in the miniature MPS mode in Fig.23(b). Comparing these photos, it is observed that the magnetosphere is inflated from an arched shape in Fig.23(a) to a rather flat shape in Fig.23(b) by the plasma injections from inside the solenoidal coil. The

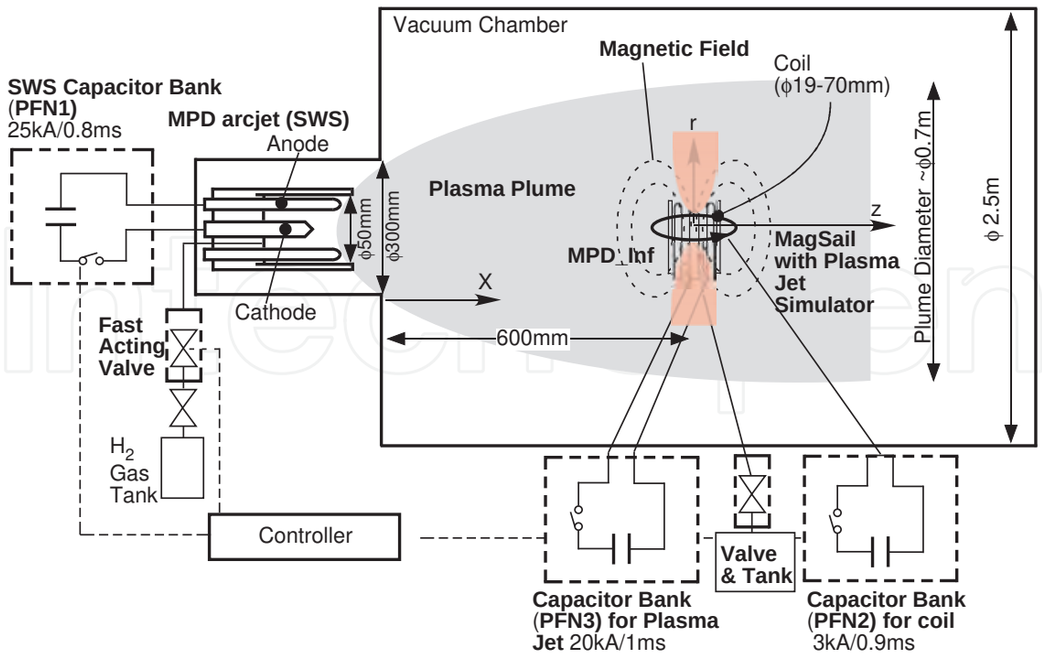

Fig. 20. Experimental setup for magnetoplasma sail (MPS).

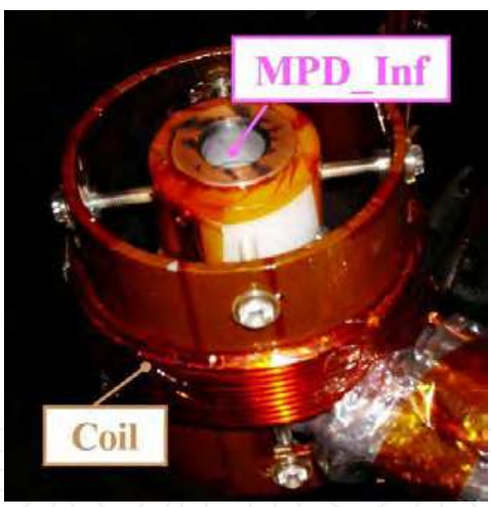

Fig. 21. Miniature MPS spacecraft (20-mm diameter MPD is installed inside 75-mm-diameter coil).

distances from the coil center to the magnetospheric boundary are 119.3 mm in Fig.23(a), and 145.3 mm in Fig.23(b); these distances are estimated from each photo. Therefore, from this evaluation, the magnetic field expansion observed is 26 mm. This is our first and successful magnetic field inflation experiment in laboratory.

Currently, experimental efforts are going on: 1) to form a large MPS magnetosphere, and 2) to detect increased thrust level by MPS operation. Direct thrust measurements of the miniature MPS is very interesting, but due to facility limitation, thrust measurement so far was not successful. Our goal is to evaluate a clear thrust gain (thrust of MPS divided by

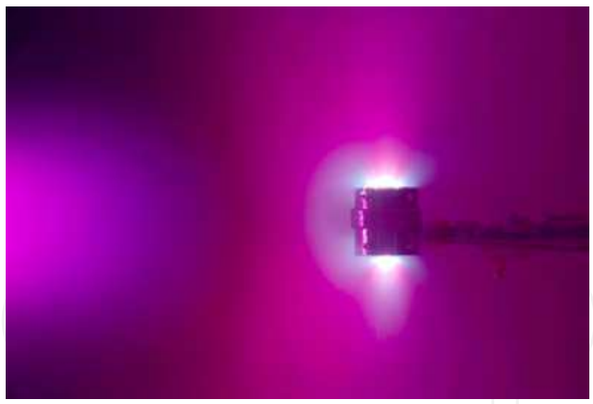

Fig. 22. Typical flow around miniature MPS during quasi-steady operation (discharge current of SWS is 8 kA (H_2;0.4 g/s), and discharge current of MPD_Inf is 4.2 kA (H_2;0.05 g/s)).

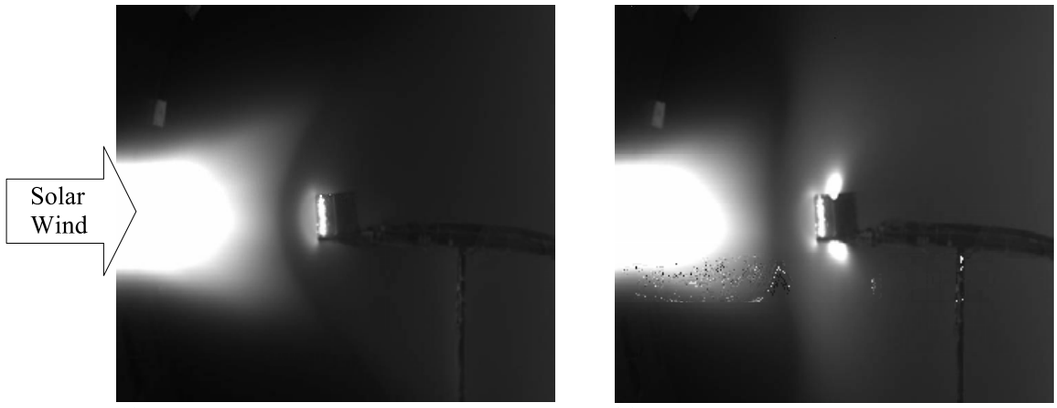

Fig. 23. Photo of scale-model experiment of MPS; a) miniature MagSail and b) miniature MPS. (simulated solar wind is introduced to 5cm/20turn coil. SWS: u_{sw}=45 km/s, n_{sw}=1.8x10^{19} m^{-3}, H_2, 0.4 g/s. From inside the coil, a plasma jet is ejected from 2-cm diameter MPD : H_2, 0.04 g/s, 0.06 T at the surface of the MPD, and J=3.5 kA for the miniature MPS).

thrust of MagSail) that is possible by MPS. For this purpose, a higher power plasma source is going replace the small (20-mm-diameter) MPD arcjet to obtain two times larger magnetic cavity size than that of MagSail. Also, several plasma sources are prepared that offer both low velocity and high velocity plasma jet. These setups will enable thrust gain more than 200%, so that an increased thrust level might be detectable.

6. Conclusion

Starting from the basic theory of sail propulsion using the solar wind, current status of solar wind sail (MPS) research, in particular experiment using a plasma wind tunnel, is described. In the experiment, using a self-field magnetoplasmadynamic arcjet as a solar wind simulator, quasi-steady interaction between a plasma flow and a magnetic cavity is obtained for a Magsail (consisting of only a coil) and for an MPS (which accomplishes an inflated magnetic cavity by a plasma jet from inside a coil). So far, thrust measurement of these sails was conducted for only a few limited cases of Magsail (without plasma jet from spacecraft),

and extension of the experimental set-up to MPS thrust measurement is still going on. During the quasi-steady interaction of about 0.8 ms, the dynamic behavior Magsail/MPS in laboratory is observed, and it was found that the magnetic cavity of Magsail is fluctuating in a frequency rage of 10-800 kHz. Thrust by Magsail is hence produced under rather turbulent plasma flow to magnetic cavity interaction.

Inspired by the ideas of MagSail and its derivatives, many new sail propulsion system are advocated. Khazanov and Akita proposed the usage of solar radiation to enhance thrust by MagSail (Khazanov et al., 2005 and Akita and Suzuki, 2004). Also, Slough proposed a way to capture the solar wind momentum by using a rotating magnetic field, and the new system is called 'the plasma magnet' (Slough, 2005). The plasma magnet is already accessed by laboratory experiment (Slough, 2007). In 2004, Janhunen proposed a completely new idea using the solar wind, which has a set of thin long wires being kept at a high positive potential so that the wires repel and deflect incident solar wind protons and it is called as electrostatic sail (Janhunen, 2004; Janhunen & Sandroos, 2007). These ideas are not so matured to proceed to a flight demonstration in space, but attractive solar wind sails that are competitive against the existing thruster technology is emerging.

7. Acknowledgment

We would like to express our acknowledgments to the members of the MPS working group (in particular, Dr. Kazuma Ueno, Mr. Yuya Oshio for providing experimental data, and Dr. Hiroyuki Nishida, Dr. Yoshihiro Kajimura, Dr. Iku Shinohara, Dr. Masaharu Matsumoto, Mr. Yasumasa Ashida, Dr. Hirotaka Otsu, Dr. Kazuhisa Fujita, and Prof. Hideyuki Usui) for their valuable activities in the analysis of MPS. This research is supported by: 1) the Grant-in-Aid for Scientific Research (A) (No.21246126) of the Japan Society for Promotion of Science, 2) the space plasma laboratory and the engineering committee of the institute of space and astronautical science in Japan Aerospace Exploration Agency (JAXA), and 3) Japan Science and Technology Agency, CREST.

8. References

Akita, D., and Suzuki, K., On the Possibility of Utilization of Radiation Pressure in Magnetic Sails, Proceedings of Symposium on Flight Mechanics and Astrodynamics, (2004), pp.1-4 (in Japanese)

Andrews, D.G., and Zubrin, R.M., Magnetic Sails and Interstellar Travel, Journal of the British Interplanetary Society, Vol.43, (1990), pp.265-272, ISSN 0007-084X

Bachynski, M.P. and Osborne, F.J.F., Laboratory Geophysics and Astrophysics, in Advances in Plasma Dynamics (Anderson, T.P. and Springer R.W. Eds), (1965). Northwestern University Press

Fujita, K., Particle Simulation of Moderately-Sized Magnetic Sails, The Journal of Space Technology and Science, Vol.20, No.2, (2004), pp.26-31, ISSN 0911-551X

Funaki, I. Kojima, H., Yamakawa, H., Nakayama, Y., and Shimizu, Y., Laboratory Experiment of Plasma Flow around Magnetic Sail, Astrophysics and Space Science, Vol.307, No.1-3, (2007), pp.63-68, ISSN 0004-640X

Funaki, I., Kimura, T., Ueno, K., Horisawa, H., Yamakawa, H., Kajimura, Y, Nakashima, H., and Shimizu, Y., Laboratory Experiment of Magnetoplasma Sail, Part 2: Magnetic

Field Inflation, Proceedings of 30th International Electric Propulsion Conference, IEPC2007-94, Florence, Sept. 2007

Frisbee, R. H., Advanced Space Propulsion for the 21st Century, Journal of Propulsion and Power, Vol.19, No.6, (2003), pp.1129-1154, ISSN 0748-4658

Giersch, L., Winglee, R.M., Slough, J., Ziemba, T., Euripides, P., Magnetic Dipole Inflation with Cascaded Arc and Applications to Mini-magnetospheric Plasma Propulsion, 39th AIAA/ASME/SAE/ASEE Joint Propulsion Conference & Exhibit, AIAA-2003-5223, Huntsville, July 2003

Janhunen, P., Electric Sails for Spacecraft Propulsion, Journal of Propulsion and Power, Vol.20, No.4, (2004), pp.763-764, ISSN 0748-4658

Janhunen, P., and Sandroos, A., Simulation Study of Solar Wind Push on a Charged Wire: Basis of Solar Wind Electric Sail Propulsion, Annales Geophysicae, Vol.25, (2007), pp.755–767, ISSN 0992-7689

Kajimura, Y., Usui, H., Ueno, K., Funaki, I., Nunami, M., Shinohara, I., Nakamura, M., and Yamakawa, H., Hybrid Particle-in-Cell Simulations of Magnetic Sail in Laboratory Experiment, Journal of Propulsion and Power, Vol.26, No.1, (2010), pp.159-166, ISSN 0748-4658

Khazanov, G., Delamere, P., Kabin, K., Linde, T. J., Fundamentals of the Plasma Sail Concept: Magnetohydrodynamic and Kinetic Studies, Journal of Propulsion and Power, Vol.21, No.5, (2005), pp.853-861, ISSN 0748-4658

Nishida, A. Ed., Magnetospheric Plasma Physics, (1982). Center for Academic Publications Japan, ISBN90-277-1345-6

Obayashi, T., Solar Terrestrial Physics (1970). Syokabo, Tokyo (in Japanese), ISBN4-7853-2405-8

Omidi, N., and Karimabadi, H., Kinetic Simulation/Modeling of Plasma Sails, 39th AIAA/ASME/SAE/ASEE Joint Propulsion Conference and Exhibit, AIAA-2003-5226, Huntsville, July 2003

Oshio, Y., Ueno, K., and Funaki, I., Fluctuation of Magnetosphere in Scale-model Experiment of Magnetic Sail, 31st International Electric Propulsion Conference, IEPC2007-94, Michigan, Sept. 2009

Slough, J., High Beta Plasma for Inflation of a Dipolar Magnetic Field as a Magnetic Sail (M2P2), Proceedings of 27th International Electric Propulsion Conference, IEPC01-202, Pasadena, Oct. 2001

Slough, J. and Giersch, L., The Plasma Magnet, 41st AIAA/ASME/SAE/ASEE Joint Propulsion Conference & Exhibit, AIAA-2005-4461, Tucson, Arizona, July 2005

Slough, J., Plasma Sail Propulsion based on the Plasma Magnet, Proceedings of 30th International Electric Propulsion Conference, IEPC2007-15, Florence, Sept. 2007

Ueno, K., Kimura, T., Ayabe, T., Funaki, I., Yamakawa, H., and Horisawa, H., Thrust Measurement of Pure Magnetic Sail, Transactions of JSASS, Space Technology Japan, Vol. 7, (2009), pp.Pb_65-Pb_69, ISSN 1884-0485

Ueno, K., Funaki, I., Kimura, T., Horisawa, H., and Yamakawa, H., Thrust Measurement of Pure Magnetic Sail using Parallelogram-pendulum Method, Journal of Propulsion and Power, Vol.25, No.2, (2009), pp.536-539, ISSN 0748-4658

Ueno, K., Oshio, Y., Funaki, I., Ayabe, T., Horisawa, H., and Yamakawa, H., Characterization of Magnetoplasma Sail in Laboratory, Proceedings of 27th

International Symposium on Space Technology and Science, ISTS-2009-b-42, Tsukuba, June 2009

Winglee, R.M., Slough, J., Ziemba, T., and Goodson, A., Mini-Magnetospheric Plasma Propulsion: Tapping the Energy of the Solar Wind for Spacecraft Propulsion, Journal of Geophysical Research, Vol.105, No.21, (2000), pp.21067-21078, ISSN0148-0227

Winglee, R.M., Ziemba, T., Euripides, P., and Slough, J., Computer Modeling of the Laboratory Testing of Mini-Magnetospheric Plasma Propulsion, Proceedings of 27th International Electric Propulsion Conference, IEPC-01-200, Pasadena, Oct. 2001

Winglee, R.M., Euripides, P., Ziemba, T., Slough, J., and Giersch, L., Simulation of Mini-Magnetospheric Plasma Propulsion (M2P2) Interacting with an External Plasma Wind, 39th AIAA/ASME/SAE/ASEE Joint Propulsion Conference & Exhibit, AIAA-2003-5224, Huntsville, July 2003

Yamakawa, H., Funaki, I., Nakayama, Y., Fujita, K., Ogawa, H., Nonaka, S., Kuninaka, H., Sawai, S., Nishida, H., Asahi, R., Otsu, H., and Nakashima, H., Magneto Plasma Sail: An Engineering Satellite Concept and its Application for Outer Planet Missions, Acta Astronautica, Vol.59, (2006), pp.777-784, ISSN 0094-5765

Ziemba, T.M., Winglee, R.M., Euripides, P., and Slough J., Parameterization of the Laboratory Performance of the Mini-Magnetospheric Plasma Propulsion (M2P2) Prototype, Proceedings of 27th International Electric Propulsion Conference, IEPC-01-201, Pasadena, Oct. 2001

Ziemba, T., Euripides, P., Winglee, R.M., Slough, J., Giersch, L., Efficient Plasma Production in Low Background Neutral Pressures with the M2P2 Prototype, 39th AIAA/ASME/SAE/ASEE Joint Propulsion Conference & Exhibit, AIAA-2003-5222, Huntsville, July 2003

Zubrin, R.M., and Andrews, D.G., Magnetic Sails and Interplanetary Travel, Journal of Spacecraft and Rockets, Vol.28, No.2, (1991), pp.197-203, ISSN 0022-4650

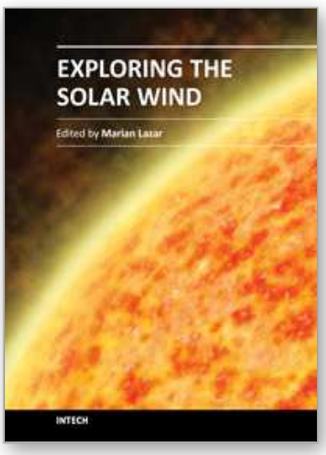

Exploring the Solar Wind

Edited by Dr. Marian Lazar

ISBN 978-953-51-0339-4
Hard cover, 462 pages
Publisher InTech
Published online 21, March, 2012
Published in print edition March, 2012

This book consists of a selection of original papers of the leading scientists in the fields of Space and Planetary Physics, Solar and Space Plasma Physics with important contributions to the theory, modeling and experimental techniques of the solar wind exploration. Its purpose is to provide the means for interested readers to become familiar with the current knowledge of the solar wind formation and elemental composition, the interplanetary dynamical evolution and acceleration of the charged plasma particles, and the guiding magnetic field that connects to the magnetospheric field lines and adjusts the effects of the solar wind on Earth. I am convinced that most of the research scientists actively working in these fields will find in this book many new and interesting ideas.

INTECH
open science | open minds

InTech Europe
University Campus STeP Ri
Slavka Krautzeka 83/A
51000 Rijeka, Croatia
Phone: +385 (51) 770 447
Fax: +385 (51) 686 166
www.intechopen.com

InTech China
Unit 405, Office Block, Hotel Equatorial Shanghai
No.65, Yan An Road (West), Shanghai, 200040, China
中国上海市延安西路65号上海国际贵都大饭店办公楼405单元
Phone: +86-21-62489820
Fax: +86-21-62489821

IntechOpen